https://doi.org/10.1016/j.ultras.2024.107289

A Single Crystal Row–Column-Array for 3D Ultrasound Imaging

Guo Li[+,*,a,b], Qiandong Sun[+,c], Yapeng Fu[c], Shilin Hou[a], Jiaming Zhang[a], K.L. Xu[*,c, d], and J.Y. Dai[*,a]

[a] Department of Applied Physics, The Hong Kong Polytechnic University, Hong Kong, China

[b] School of Automation, Xi'an University of Posts &Telecommunications, Xi'an,China

[c] Department of Biomedical Engineering, Fudan University, Shanghai, China.

[d] Shanghai PodaMed Medical Technology Co., Ltd. China.

[*]Corresponding Authors: liguo@xupt.edu.cn; xukl@fudan.edu.cn ; jiyan.dai@polyu.edu.hk

Abstract— In vivo 3D ultrasound imaging with 2D-array transducers is of great importance for both clinical application and biomedical research, but it is complicated in fabrication and also very expensive in hardware due to thousands of electronic channels. In this work, we demonstrate a new fabrication process of 7-MHz 128+128 elements row-column-array (RCA) transducer with relaxor ferroelectric PMN-0.28PT single crystal. With piezoelectric single crystal and improved acoustic matching, the optimized performance of -6 dB bandwidth of ~82% and insertion loss of -44.6 dB is achieved. The axial and lateral imaging resolutions at different depth of the RCA transducer are quantified by the point spread function (PSF), and the results are respectively 0.20 mm and 0.41 mm at the depth of 7.7 mm, and 0.22 mm and 0.47 mm at the depth of 16.7 mm. The transducer was validated experimentally on a hyperechoic phantom, and 3D view and slices of B-mode images were obtained. The experimental results indicate that our developed RCA transducer can obtain high-quality 3D ultrasound images, demonstrating great potential on ultrafast 3D and functional imaging.

***Index Terms*—Biomedical imaging, Biomedical transducers, Ferroelectric devices, Ultrasonic transducer arrays**

I. INTRODUCTION

Due to its fast acquisition, non-destructive and non-ionizing radiation characteristic as opposed to other diagnostic modalities, ultrasound imaging is a popular diagnostic tool for clinical and veterinary medicine, [1-6]. Recent advances show the development trend of miniature, high frequency and volumetric imaging benefited from the rapid improvement of manufacturing technique of transducers and computing power [7-9]. As a major innovation in ultrasound imaging technologies, 3D ultrasound imaging has several advantages over 2D ultrasound, such as orientations and slices determination, more accurate volume measurements, and improved detection of cystic or cancerous masses which are not available for 2D ultrasound [10]. The traditional 3D imaging method based on fully sampled 2D arrays often requires a large number of electronic channels which limit the aperture size and imaging resolution in application. Alternatively, row-column addressing (RCA) matrix was originally presented in by Morton and Lockwood in 2003, which are composed of two sets of orthogonal vertical and horizontal overlapping transducers which effectively reduces the number of elements from N^2 to 2N [11,12]. Due to significant reduction of the number of electronic channels and data storage and processing requirements, RCA arrays have been demonstrated in application for 4D ultrafast imaging, 3D functional imaging and super-resolution imaging in recent years. Christiansen *et al*. have demonstrated the fabrication, characterization, and experimental imaging results of a row–column-addressed capacitive micromachined ultrasonic transducer (CMUT) RCA array with 62+62 element λ/2-pitch and integrated apodization in 2015 [13]. In 2018, Engholm *et al*. investigated compound lenses for RCA ultrasound transducers for increasing the field-of-view to a curvilinear volume region, while retain a flat sole to avoid trapping air between the transducer sole and the patient, which would otherwise lead to unwanted reflections [14]. Sauvage *et al*. developed the orthogonal plane wave (OPW) compounding strategy for 4D ultrafast imaging using RCA array in 2018 [15], and in 2020, a 4D vascular brain image at high volume rate using 15 MHz RCA probe of 128+128 channels was achieved [16]. In 2020, Jensen *et al*. presented a 3D super-resolution pipeline using a 3 MHz RCA array [17], and then realized the tensor velocity imaging using the transverse oscillation cross-correlation estimator based on a 128+128 RCA probe in 2023[18]. Xu *et al* have investigated the multi-angle OPW method for 3D blood flow imaging using an RCA matrix with 128+128 RCA array, centered at 6 MHz [19], and then proposed a novel beamforming method to improve the resolution of RCAs [20]; Jørgensen *et al.* have proposed a fast beamforming method for 3D volume imaging of RCA arrays, with a negligible difference in image quality compared to conventional beamforming approach, which demonstrated that RCA arrays have great potential on 3D real time imaging [21].

It is well-known that the ultrasound imaging quality depends on the performance of transducer, and the approaches to improve the performance include the improved piezoelectric properties of the active layer and

acoustic matching in an ultrasound transducer. In this work we adopt single crystal relaxor ferroelectric material $Pb(Mg_{1/3}Nb_{2/3})O_3$-0.28$PbTiO_3$ (PMN-0.28PT) as the piezoelectric material which is an excellent candidate for the active layer due to the presence of polar nanoregions (PNRs) [22-26]. The relaxor ferroelectric single crystal at a morphotropic phase boundary (MPB) possesses much higher ferroelectricity, piezoelectric constant (d_{33}≥2000 pC/N), dielectric constant and electromechanical coupling factor (k_{33}~0.92) compared to non-relaxor based materials such as PZT [27-32]. However, the relaxor PMN-0.28PT single crystal has disadvantages such as low ferroelectric phase transition temperature (T_m) and low coercive field (E_C), leading to the low stability of polarization. Consequently, a PMN-0.28PT-based transducer requires a more stringent temperature control and an additional pre-driving DC voltage to retain its polarization and device performance [33,34]. Moreover, the single crystal has a brittle nature that increases the difficulty of developing 2D array transducers and reduces the uniformity and yield rate of final product. In this work, beyond adopting PMN-0.28PT single crystal, we also develop a new electrode connection process enabling excellent acoustic matching, and therefore, demonstrate successful fabrication of a 7-MHz 128+128 elements RCA transducer with very good performance. The resolutions of the developed transducer and the demonstration of in vitro phantoms imaging are presented. The results show a feasible way of manufacturing single crystal-based RCA transducers for ultrafast 3D imaging.

II. TRANSDUCERS FABRICATION

As shown in Fig. 1 (a), the structure of our transducer has three layers, i.e. a double matching layer with the thickness of a quarter wavelength each, a piezoelectric layer, and a backing layer. The outlook of our fabricated RCA transducer is shown in Fig. 1(b). In our transducer, PMN-0.28PT plate (Shanghai Institute of Ceramics, The Chinese Academy of Sciences, Shanghai, China) was selected as the piezoelectric layer owing to its excellent piezoelectric properties [35] listed in Table 1. According to Gregg et al. at 1969 [36], the acoustic impedance of PMN-0.28PT is Z_p = 32 MRayl and that of human organs is Z_l = 1.65 MRayl, The value of single matching can be easily achieved, however, the single matching layer has a slightly lower sensitivity and bandwidth comparing with double and triple matching schemes. Even the double and triple matching schemes are much better than single layer matching for transducer's performance, they are more difficult to be optimized since the first layer of them needs high acoustic impedance, especially for the triple matching scheme [35]. Therefore, double matching scheme was chose in this product, where the required acoustic impedances of the first (Z_1) and second (Z_2) matching layers are calculated by equations (1) and (2):

$$Z_1 = Z_p^{\frac{4}{7}} Z_l^{\frac{3}{7}} \qquad (1)$$

$$Z_2 = Z_p^{\frac{1}{7}} Z_l^{\frac{6}{7}} \qquad (2)$$

In these equations, Z_p and Z_l are the impedances of piezoelectric layer and loading medium, respectively. The calculated acoustic impedances of the first and second matching layers are 8.98 and 2.52 MRayl, respectively.

Table 1 Properties of PMN-28%PT single crystal.

Longitude velocity	4038 m/s
Density	7920 kg/m^3
Acoustic impedance	32 MRayl
Piezoelectric constant (d_{33})	1400 pC/N
Clamped dielectric constant (ε_{33}^S)	1200
Electromechanical coupling coefficient (k)	0.85
Loss tangent	0.005

In our transducer, the first matching layer is a mixture of alumina power (Buehler Inc., Illinois, U.S.A.) and epoxy (Insulcast 502, ITW Insulcast, U.S.A) with the acoustic impedance of 8.5 MRayl using the high compression fabrication method presented by our group earlier [37].The very high acoustic impedance value and very low attenuation make this matching material superior, and therefore, can enhance the performance of the ultrasound transducers, especially for medical imaging applications. The second matching layer is Epoxy 301 with an acoustic impedance of 3.0 MRayl. A mixture of Al_2O_3 powder Epoxy 301 was utilized as the backing layer due to its acoustic attenuation over a wide frequency range. The acoustic impedance of mixture 1-2 μm Al_2O_3 powder + Epoxy 301 is 6.7 MRayl. The properties of matching and backing layers are summarized in Table 2.

Table 2 Properties of matching and backing layers.

Matching layer number	1	2	Backing layer
Material	1-2 μm Al_2O_3 powder + Epoxy 502 Compressed	Epoxy 301-1	1-2 μm Al_2O_3 powder + Epoxy 301-1
Weight ratio	2:1	N/A	2:1
Acoustic impedance (MRayl)	8.3	3.0	6.7
Velocity (ms^{-1})	3395	2650	3302
Density (kgm^{-3})	2449	1132	2030

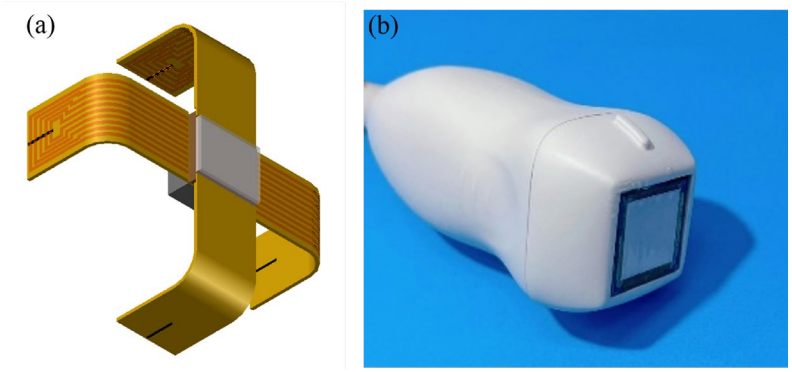

Fig. 1(a) Schematic diagram of the designed RCA transducer, and (b) outlook of the transducer probe.

To optimize transducer performance, the parameters of different layers were used to simulate the two-way acoustic pulse echo response in time and frequency domains with PiezoCAD (Sonic Concepts, Woodinville, WA) based on the Krimholtz, Leedom and Matthaef (KLM) model [38,39]. The properties of the layers in simulation model are set as Table 1. The acoustic loads, matching layers, piezoelectric layer and backing layer were modeled successively, and the free boundary conditions were used in the model. By optimizing the pulse amplitude and bandwidth, the thickness of each layer was determined, and the optimized specifications of the transducer are listed in Table 3. Those dimensions were used to fabricate the RCA in this study. The center frequency of the transducer was designed as 7.3 MHz and the pitch of array was set as 120 μm which is 0.58 λ of the center frequency. The electrical input impedance and pulse-echo impulse response of simulation is shown in Figs. 2 (a) and (b), respectively. In Fig. 2 (a), the electrical input impedance vs frequency curve presents two resonances with minimum impedance at 4.6 MHz and 9.0 MHz, which contribute to two peaks of the pulse-echo impulse at 5.1 MHz and 9.0 MHz shown in Fig. 2(b), respectively. Pulse-echo impulse response achieves the -6 dB bandwidth 89% at the center frequency 7.3 MHz.

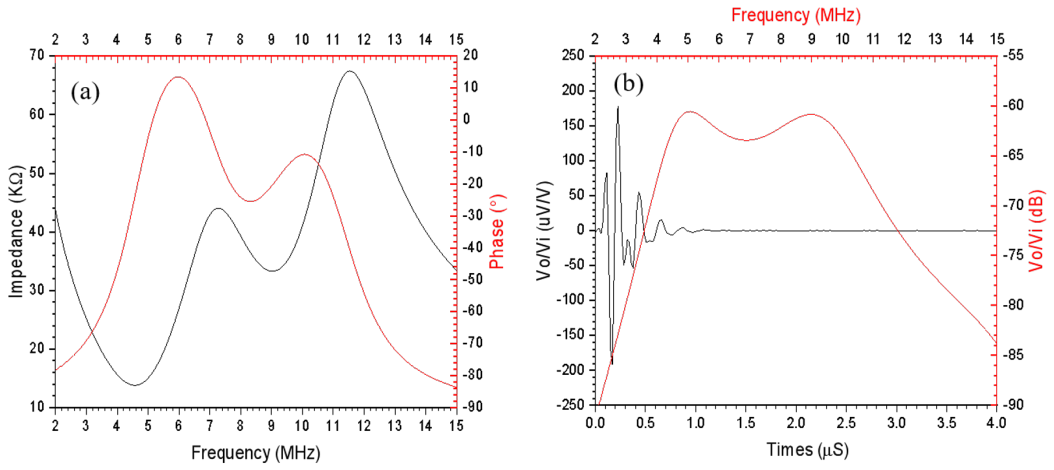

Fig. 2 PIEZOCAD simulation of a single element: (a) electrical impulse impedance and phase, and (b) pulse-echo impulse response.

Table 3 Specifications of the designed RCA transducer

Designed center frequency	7.3 MHz
Number of elements	128x128
Pitch	120 μm (0.58 λ)
Elements width	90 μm
Row/column length	15.36 mm
Kerf width	30 μm
PMN-PT thickness	190 μm
First matching layer thickness	88 μm
Second matching layer thickness	48 μm
Backing layer thickness	5 mm

The PMN-0.28PT single crystal plate with the dimensions of 20×20×0.5 mm^3 was waxed on a glass plate and polished by 4000 grit alumina polishing powder. The specimen was then diced into 128 elements along row direction using a 0.025 mm-width hub blade (ZHZZ series, DISCO Co. Ltd., Omori-Kita, Japan) with the spindle rotation speed of 20000 rpm and the feeding speed of 0.4 mms^{-1}. The kerfs were then filled by epoxy EPO-TEK 301-1, and after curing at room temperature for 24 hours, the crystal was diced along column direction and filled with epoxy again. Subsequently, the surface of the array was grinded to remove the excess epoxy and polished with 4000 grit alumina powder. Then, a Cr/Cu/Au tri-layered electrode with thicknesses of 25, 1000 and 50 nm, respectively, was sputter deposited on the surface of polished PMN-PT single crystal. This layer of electrode is critical for the success of the transducer fabrication since the connection across elements through epoxy filled kerfs are easily broken. So, the flatness of elements with epoxy kerfs and the adhesion of the electrode on the elements should be strictly controlled.

After second dicing on the surface of the epoxy-filled kerfs to separate two rows, two opposite direction PCB were adhered alternately to the two ends of separated electrodes, finishing the connection from the active elements to metal contact leads. Two custom-designed flexible circuits (FPCs, Shenzhen HongRuiKang electronics co. ltd., Shenzhen, China) with 64-electrode-traces were adhered to the front surface of array on both sides by injecting an epoxy between the FPC and edge of the active elements with separated electrodes. The electrode pads of the FPCs were aligned and mounted to the array under an optical microscope, where a fixture was used to compress the pads to enhance the adhesion and minimize the contact resistance. Connecting the FPC on both sides instead of one side not only minimizes the manufacturing difficulty (electrode trace separation can be doubled), but also reduces the electrical cross-talk between adjacent

elements [40]. The array with two PCBs was casted with the mixture of 1-2 μm Al_2O_3 powder and Epoxy 301-1 as backing layer, and then the array with backing layer was turned over and adhered to the glass plate and then lapped down to 200 μm followed by polishing and coating of the same electrode layer. After repeating the polishing and dicing process, two opposite directions of PCB were adhered alternately to the two ends of separated electrodes, finishing the connection of column active elements to the metal contact leads.

The double matching layers were then adhered to the surface of the array to finish the whole transducer fabrication process. The first matching layer was prepared using our invented method, i.e. a process analogous to making a ceramic plate of a mixture of fine alumina powder and epoxy 502 with extremely high content of alumina (higher than 66 wt%) by adding a hydraulic pressure of 62.4 MPa. The high-pressure compression results in a significant increase of acoustic impedance of 8.54 MRayl [41,42], which is comparable to the heavy metal constituted matching but with much lower attenuation. Most importantly, the enhancement is mainly contributed by the acoustic velocity instead of the density, which allows the broader tolerance of thickness especially in high frequencies. In addition, the 1-2 μm alumina powder is much smaller than the acoustic wavelength such that the scattering effect can be minimized to reduce the attenuation at the designed center frequency [40,43]. The first matching layer of ~106 μm thick (according to the simulation results in Table 2) was adhered on the front surface of the array using M-bond 610. A 66 μm-thick vacuum degassed Epoxy 301-1 was coated on the first matching layer. Finally, the transducer was installed into the housing with cables connected. The PMN-PT-based RCA transducer prototype is shown in Fig. 3(a), and detailed layers thicknesses and dimensions are shown in Fig. 3(b). The thicknesses of PMN-PT, first matching layer and second matching layer are 190, 88 and 48 μm, respectively. The thickness of backing layer depends on the attenuation at the corresponding center frequency.

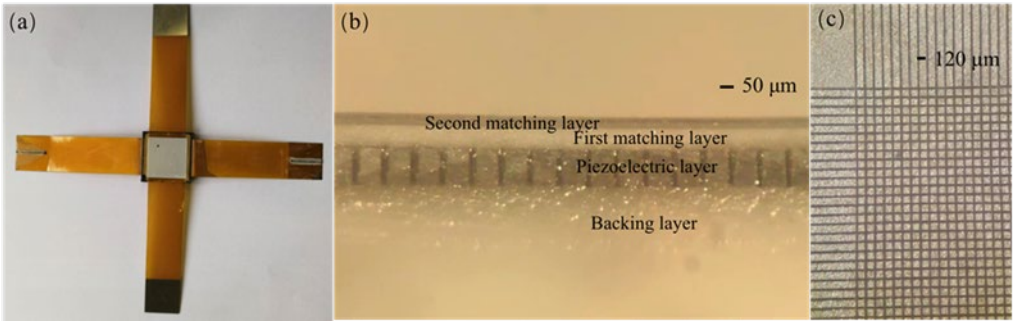

Fig. 3 (a) Top view of the fabricated RCA transducer, (b) cross-sectional view of the RCA elements showing two-layer matching, and (c) top view of the RCA elements without matching layer.

III. TRANSDUCER PERFORMANCE

A. Electrical and acoustic characteristics

First, the basic performance of the transducer was characterized by a 4294A precision impedance analyzer (Agilent Technologies Inc. Philadelphia, PA). As single element representative results shown in Fig. 4, the impedance and phase diagrams of the nine single elements of the transducer have a clean thickness resonance of around 7.1 MHz and electrical impedance of around 150 Ω at the resonance frequency. Based on Eq. (3), effective electromechanical coupling coefficient k_{eff} can be calculated to be 0.60 according to the IEEE standard [44], where f_r is the resonance frequency at which the impedance reaches the minimum and f_a is the anti-resonance frequency at which the impedance reaches the maximum. Impedance and phase diagrams of all rows and columns are shown in Fig. 5, where most of the rows and columns have a resonance of around 7.5 MHz and anti-resonance of around 10 MHz from which the effective electromechanical coupling coefficient k_{eff} can be calculated to be 0.66. It's worth noting that the RCA impedances were measured by connecting 0.5 m long flexible PCB, so in our PiezoCAD simulation, 0.85 of k_{eff} which is more close to k_{33} (our element dimension has aspect ratio of 2.1) of PMN-PT single crystal was used and the calculated bandwidth is 89%.

$$k_{eff} = \sqrt{\frac{f_a^2 - f_r^2}{f_a^2}} \qquad (3)$$

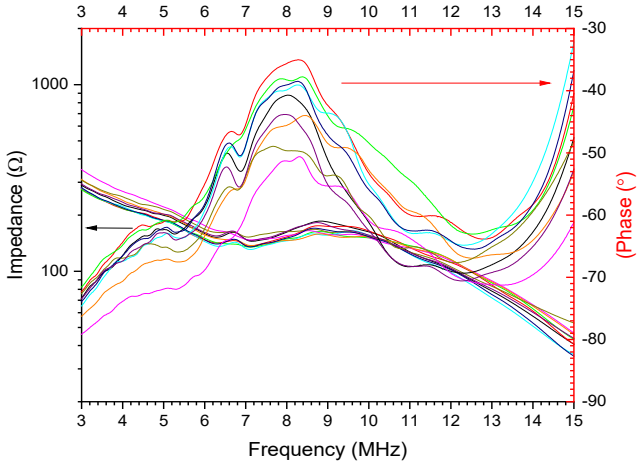

Fig. 4 Electrical impedance-phase angle versus frequency of nine representative single elements

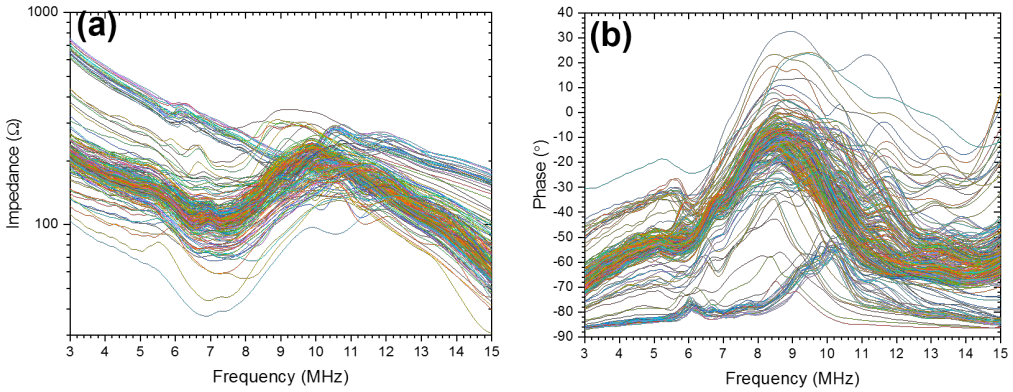

Fig. 5 Electrical impedance (a) and phase angle (b) versus frequency for all rows and columns

In the two-way pulse-echo measurement, the transducer elements immersed in water were individually excited by a Panametrics 5900PR pulser/receiver of 4 μJ energy at the repetition frequency of 200 Hz. A thick stainless-steel block was used as reflector in water. The electrical coupling, gain and attenuators of the equipment were set as 50 Ω, 26 dB, and 15 dB, respectively. A fast Fourier transform (FFT) in the mathematical function of the oscilloscope was operated to transform the time domain signals into frequency domain spectra. It's worth noting that the RCA pulse-echoes were measured by connecting 1.5 m long coaxial cable. Fig. 6 shows the pulse-echo responses of the nine single elements of the transducer, where one can see that the pulse-echo responses present an averaged peak-to-peak amplitude of 254 mV with pulse echo time 21μs and a center frequency of 6.4 MHz. There are three main factors contributing to the differences to the simulated center frequency. Firstly, in the single element of RCA fabrication, the matching layers are not divided into separate elements, so the piezoelectric elements are surrounded by epoxy. Secondly, the dimensional control of thickness direction in the RCA fabrication process is not precise, so the thickness of the bonding layer cannot be ignored.

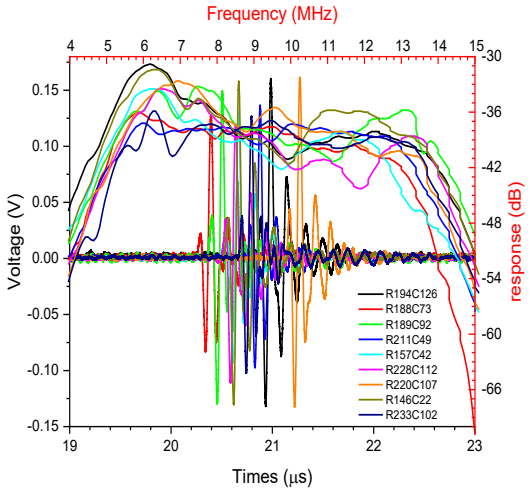

Fig. 6 Pulse-echo signal and frequency spectrum of nine representative single elements

Fig. 7 (a) shows the pulse-echo responses of a representative row or column of the transducer. The pulse-echo response presents an representative peak-to-peak voltage amplitude of 1.12 V and a -6 dB bandwidth of ~82% from 5.1 to 12.2 MHz at a center frequency of 8.7 MHz. Fig. 7(b) shows the peak-to-peak voltage amplitude from pulse-echo responses of all rows and columns, and we can see that almost all peak-to-peak voltage amplitudes range from 0.6 to 0.8 V.

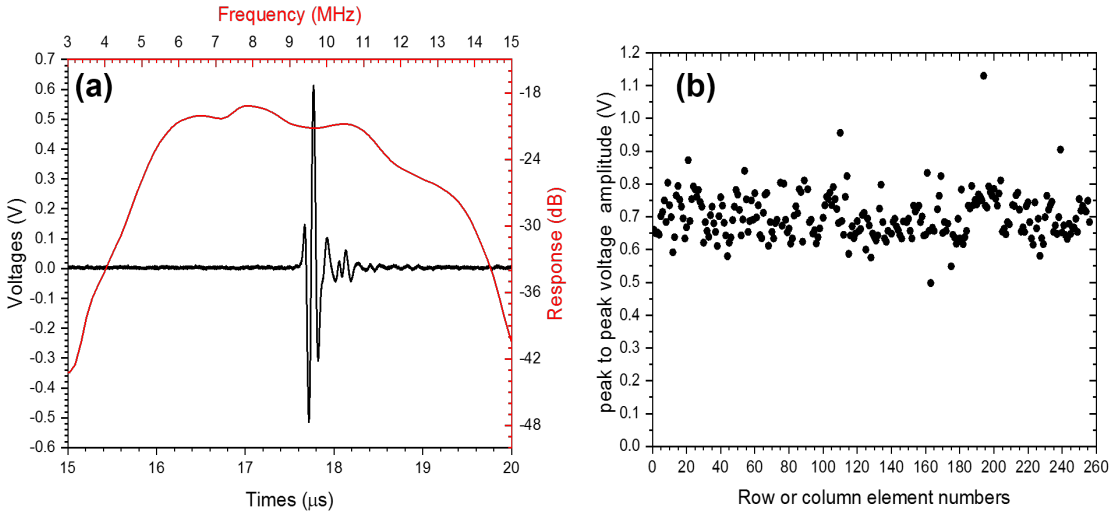

Fig. 7 (a) A representative row or column pulse-echo signal and frequency spectrum, and (b) pulse-echo peak-to-peak voltage amplitudes of 128 rows and 128 columns.

Finally, insertion loss (IL) of the transducer was measured to evaluate its sensitivity. During the measurement, the front side of transducer was immersed in water and excited by a waveform in a tone burst mode with a signal generator (AFG3251, Tektronix, Beaverton, U.S.A) with ten cycles at the center frequency of transducer. The pulse ultrasound wave was reflected by a 40 mm-thick stainless-steel block in water at a distance of 15 mm away from the transducer, and the pulse echo signal V_o was displayed on the oscilloscope (HP Infinium DSO-S 204A, Keysight Technologies Inc., Santa Rosa, CA) together with exciting burst amplitude V_i. The representative ten rows or columns and three single elements were measured. Based on Eq. (4), the calculated average insertion losses of rows/columns and single element are ~44.6 dB and ~48.1, respectively.

$$IL = -20log\left(\frac{V_o}{V_i}\right) \qquad (4)$$

B. Imaging performance

The imaging performance was evaluated through the copper wires of 0.01 mm diameter as scattering target for PSF study and the multi-purpose multi-tissue ultrasound phantom (CIRS, Model 040GSE). The 6 copper wires were fixed at different depth in a box filled with water. The box sides were covered with

acoustical absorbing material to reduce the boundary reflection. The hyperechoic lesions were all of a 8 mm diameter. The measurements were performed with our RCA probe connected to a Verasonics Vantage 256 research scanner. During imaging, the steering angles were set as 15 angles with a span of 30°, corresponding to a pulse reception frequency (PRF) of 4.5 KHz.

The orthogonal plane wave (OPW) compounding beamforming method [45] was implemented. More specifically, the transmit and receive travel time was calculated with respect to the closest distance between the sampling pixel in 3D space and the elements; this method has been proved by Field II simulation in [19]. A Hann apodization was used for the receiving arrays to reduce the edge effects and further improve the contrast. Before the beamforming process, the IQ decomposition was implemented on the RF data. The space of reconstruction volume along the *x*-, *y*- and z-directions were all λ/2. The beamforming was performed on graphical processing units and were coded using CUDA C language within a Matlab (2021a, The MathWorks Inc., Natick, MA, USA) interface. The complete image acquisition including beamforming and 3D reconstruction requires a total time shorter than 15s. The 3D reconstruction results and slices along the *x*- and *y*-directions of PSF are shown in Fig. 8 (a). We quantified the intensity distribution along the depth and transverse direction of three chosen scattering targets in Fig. 8 (a), and then the axial and lateral -6 dB resolution were determined to be 0.20 mm and 0.41 mm at depth of 7.7 mm, 0.22 mm and 0.47 mm at depth of 16.7 mm, and 0.28 mm and 0.62 mm at depth of 26.5 mm, respectively. Fig. 8(b) shows the B-mode images of hyperechoic phantom with a clear edge, showing great performance on the image contrast and resolution.

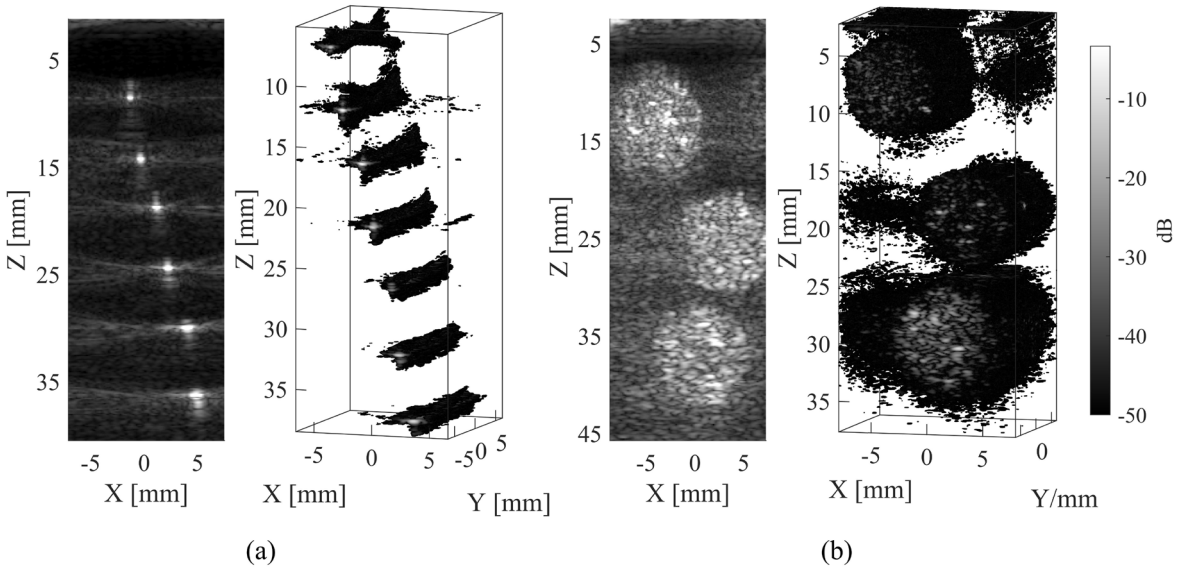

Fig. 8. 3D imaging results of copper wires (a), and cyst phantom (b).

IV. CONCLUSION

In this work, we have demonstrated the feasibility of our RCA transducer fabrication process with relaxor ferroelectric PMN-0.28PT single crystal. Our developed 128+128 elements 7-MHz RCA transducer has wide -6 dB bandwidth of ~82%, benefited from excellent acoustic matching with ultrathin electrode layers. In vitro experiment, the axial and lateral imaging resolutions of the transducer are determined to be 0.20 mm and 0.41 mm, respectively, and 3D images of hyperechoic cyst are obtained, demonstrating the potential application of our developed single crystal array transducer for biomedical and future clinical research, such as 3D ultrasound imaging.

ACKNOWLEDGEMENTS

We acknowledge support from National Key Research and Development Program of China (Grant No. 2023YFC2410900), Guangdong-Hong Kong-Macao Joint Laboratory for Photonic-Thermal-Electrical Energy Materials and Devices (GDSTC No. 2019B121205001) and The Hong Kong Polytechnic University internal grant (UAEZ and ZVSQ). National Key Research and Development Program of China (2018YFC01163, 2018YFA0701400), National Natural Science Foundation Grants of China (62022086, 11874382, 81927808, 12104369), Shenzhen Research Grant (JCYJ20200109114237902, SGDX2020110309400200, and ZDSYS201802061806314), Youth Innovation Promotion Association CAS 2018391, CAS research projects (QYZDB-SSW-JSC018), Research funding of Guangdong Province (2020B1111130002 and 2020B1212060051) and Guangdong Special Support Program. Hong Kong Research Impact Fund (R5029-19), Hong Kong General Research Fund (15220920), HSL acknowledges support from International Collaboration project (No. 121631KYSB20190026), NSFC grant (No. 11827808, 12174415) and Guangdong Special Support Program. We acknowledge the senior artisan Kai-Hong Ho, Department of Applied Physics, The Hong Kong Polytechnic University, who made the extremely effective mechanical molds and assemblies that were instrumental in allowing the work to be completed successfully.

REFERENCES

[1] D.H. Turnbull, In utero ultrasound backscatter microscopy of early-stage mouse embryos, computerized medical imaging and graphics. 23 (1999) 25–31.

[2] G.R. Lockwood, D.H. Turnball, D.A. Christopher, F.S. Foster, Beyond 30 MHz [applications of high-frequency ultrasound imaging], engineering in medicine and biology magazine, IEEE Engineering in Medicine and Biology Magazine. 15 (1996) 60–71.

[3] C. Passmann, H. Ermert, A 100-mhz ultrasound imaging system for dermatologic and ophthalmologic diagnostics, IEEE Trans. Ultrason., Ferroelect., Freq. Contr. 43 (1996) 545–552.

[4] G.C. Kagadis, G. Loudos, K. Katsanos, S.G. Langer, G.C. Nikiforidis, In vivo small animal imaging: current status and future prospects, Medical Physics. 37 (2010) 6421–6442.

[5] J.S. Lewis, S. Achilefu, J.R. Garbow, R. Laforest, M.J. Welch, Small animal imaging: current technology and perspectives for oncological imaging, Eur J Cancer. 16 (2002) 2173-88.

[6] R.S. Jaiswal, J. Singh, G.P. Adams, High-resolution ultrasound biomicroscopy for monitoring ovarian structures in mice, Reprod Biol Endocrinol. 7 (2009) 1–7.

[7] D.R. Dietz, M.J. Fife, L.J. Busse, S. Azim, C.G. Oakley, W.M. Glenn, Laparoscopic Ultrasound for Minimally Invasive Surgery, IEEE Ultrasonics Symposium. 1995, pp. 1575–1583.

[8] Z. Pilecki, B. Koczy, M. Mielnik, G. Pilecki, J. Dzielicki, W. Jakubowski, Podstawowe techniki preparacyjne w sonochirurgii, Journal of Ultrasonography. 14 (2014) 171–178.

[9] E.A. Minnard, K.C. Conlon, A. Hoos, E.C. Dougherty, L.E. Hann, M.F. Brennan, Laparoscopic ultrasound enhances standard laparoscopy in the staging of pancreatic cancer, Annals of Surgery. 228 (1998) 182–187.

[10] A. Fenster and D.B. Downey, 3-D ultrasound imaging: A review, IEEE Engineering in Medicine and Biology Magazine. 15 (1996) 41-51.

[11] C.E. Morton, G.R. Lockwood, Theoretical assessment of a crossed electrode 2-D array for 3-D imaging, in: Proc. IEEE Ultrasonics Symposium. 1 (1995) 968-71.

[12] M. Flesch, M. Pernot, J. Provost, G. Ferin, A. Nguyen-Dinh, M. Tanter and T. Deffieux, 4D in vivo ultrafast ultrasound imaging using a row-column addressed matrix and coherently-compounded orthogonal plane waves, Phys. Med. Biol. 62 (2017) 4571–4588.

[13] Thomas Lehrmann Christiansen, Morten Fischer Rasmussen, Jan Peter Bagge, Lars Nordahl Moesner, Jørgen Arendt Jensen, and Erik Vilain Thomsen, 3-D imaging using row–column-addressed arrays with integrated apodization—part ii: Transducer fabrication and experimental results, IEEE Transactions on Ultrasonics, Ferroelectrics, and Frequency Control. 62(2015) 959-971.

[14] M. Engholm, C. Beers , H. Bouzari, J.A. Jensen, E.V. Thomsen, Increasing the field-of-view of row–column-addressed ultrasound transducers: implementation of a diverging compound lens, Ultrasonics. 88 (2018) 97–105.

[15] J. Sauvage1, M. Flesch, G. Férin, A. Nguyen-Dinh, J. Porée, M. Tanter, M. Pernot and T. Deffieux, A large aperture row column addressed probe for in vivo 4D ultrafast doppler ultrasound imaging, Phys. Med. Biol. 63(2018) 215012.

[16] J. Sauvage，T. Deffieux，J. Poree，C. Rabut and M. Pernot, 4D functional imaging of the rat brain using a large aperture row-column array, IEEE Transactions on Medical Imaging. 39 (2020) 1884-1893.

[17] J. A. Jensen et al., Three-dimensional super-resolution imaging using a row–column array, IEEE Transactions on Ultrasonics, Ferroelectrics, and Frequency Control. 67 (2020) 538-546.

[18] L.T. Jørgensen, M.B. Stuart, J.A. Jensen, Transverse oscillation tensor velocity imaging using a row–column addressed array: Experimental validation, Ultrasonics. 132(2023).

[19] Y. Fu, Q. Sun, B. Li, D. Ta, K. Xu, Three-dimensional ultrafast ultrasound imaging of blood flow using row-column addressing matrix:A simulation study, Acta Physica Sinica. 72 (2023) 074302-1.

[20] Q. Sun, Y. Fu and K. Xu, X-FMAS Beamforming Method for 3D Imaging Using Row-Column Addressed Array, in: Proc. IEEE Ultrasonics Symposium, (2023) 1-3.

[21] L.T. Jørgensen, S.K. Præsius, M.B. Stuart and J.A. Jensen, Row–column beamformer for fast volumetric imaging, IEEE Transactions on Ultrasonics, Ferroelectrics, and Frequency Control. 70 (2023) 668-680.

[22] Relaxor Ferroelectrics, Ferroelectrics. 76 (1987) 241–267.

[23] A.A. Bokov, Z.G. Ye, Recent progress in relaxor ferroelectrics with perovskite structure, J Mater Sci. 41 (2006) 31–52.

[24] W. Kleemann, Relaxor ferroelectrics: Cluster glass ground state via random fields and random bonds, Physica Status Solidi (B). 251 (2014) 1993–2002.

[25] F. Li, T. Yang, Z. Xu, N. Zhang, G. Liu, J. Wang, et al., The origin of ultrahigh piezoelectricity in relaxor-ferroelectric solid solution crystals, Nature Communications. 7 (2016) 1–9.

[26] V. Westphal, W. Kleemann, M.D. Glinchuk, Diffuse phase transitions and random-field-induced domain states of the "relaxor" ferroelectric PbMg1/3Nb2/3O3, Phys. Rev. Lett. 68 (1992) 847–850.

[27] S.-E. Park, T.R. Shrout, Ultrahigh strain and piezoelectric behavior in relaxor based ferroelectric single crystals, J. Appl. Phys. 82 (1997) 1804–1811.

[28] C.G. Oakley, M.J. Zipparo, Single Crystal Piezoelectrics: A revolutionary development for transducers, IEEE Ultrasonics Symposium. 1157–1167.

[29] R. Zhang, B. Jiang, W. Cao, Elastic, Piezoelectric, and dielectric properties of multidomain 0.67Pb(Mg1/3Nb2/3)O3–0.33PbTiO3 single crystals, J. Appl. Phys. 90 (2001) 3471–3475.

[30] S.E. Park, T.R. Shrout, Characteristics of relaxor-based piezoelectric single crystals for ultrasonic transducers, IEEE Transactions on Ultrasonics, Ferroelectrics, and Frequency Control. 44 (1997) 1140–1147.

[31] Q. Su, B. Zhu, J.H. Lee, Z. Bi, K. Shung, Q. Zhou, et al., Self-separated PZT thick films with bulk-like piezoelectric and electromechanical properties, Journal of Materials Research. 26 (2011) 1431–1435.

[32] H. Jaffe, D.A. Berlincourt, Piezoelectric transducer materials, Proceedings of the IEEE. 53 (1965) 1372–1386.

[33] J. Chen, R. Panda, Review: commercialization of piezoelectric single crystals for medical imaging applications, IEEE Ultrasonics Symposium. 2005,235–240.

[34] S. Zhang, F. Li, High performance ferroelectric Relaxor-PbTiO3 single crystals: status and perspective, J. Appl. Phys. 111 (2012) 031301.

[35] C. Wong, Y. Chen, H. Luo , J. Dai, K.H. Lam, H.L. Chan, Development of a 20-MHz wide-bandwidth PMN-PT single crystal phased-array ultrasound transducer, Ultrasonics. 73 (2017) 181-186.

[36] E.C. Grecc, G.L. Palagallo, Acoustic impedance of tissue, Investigative Radiology. 4 (1969) 357.

[37] C. Wong, S. Chan ,W. Wu, C. Suen , H.Yau, D. Wang, S. Li, J. Dai, Tunable high acoustic impedance alumina epoxy composite matching for high frequency ultrasound transducer, Ultrasonics. 116 (2021) 106506.

[38] R. Krimholtz, D.A. Leedom, G.L. Matthaei, New equivalent circuits for elementary piezoelectric transducers, Electron. Lett. 6 (1970) 398.

[39] S. Sherrit, S.P. Leary, B.P. Dolgin, Y. Bar-Cohen, Comparison of the mason and KLM equivalent circuits for piezoelectric resonators in the thickness mode, EEE Ultrasonics Symposium. 2 (1999) 921–926.

[40] A. Bezanson, R. Adamson, J.A. Brown, Fabrication and performance of a miniaturized 64-element high-frequency endoscopic phased array, IEEE Transactions on Ultrasonics, Ferroelectrics, and Frequency Control. 61 (2014) 33–43.

[41] H. Wang, T. Ritter, W. Cao, K.K. Shung, High frequency properties of passive materials for ultrasonic transducers, IEEE Transactions on Ultrasonics, Ferroelectrics, and Frequency Control. 48 (2001) 78–84.

[42] Q. Zhou, J. Cha, Y. Huang, R. Zhang, W. Cao, K.K. Shung, Alumina/epoxy nanocomposite matching layers for high-frequency ultrasound transducer application, IEEE Transactions on Ultrasonics, Ferroelectrics, and Frequency Control. 56 (2008) 213–219.

[43] M. Lukacs, J. Yin, G. Pang, R. Garcia, E. Cherin, R. Williams, et al., Performance and characterization of new micromachined high-frequency linear arrays, IEEE Transactions on Ultrasonics, Ferroelectrics, and Frequency Control. 53 (2006) 1719–1729.

[44] IEEE standard on piezoelectricity, ANSI/IEEE Std. 176-1987. New York: IEEE, 1987.

[45] M. F. Rasmussen, T. L. Christiansen, E. V. Thomsen and J. A. Jensen, 3-D imaging using row-column-addressed arrays with integrated apodization - part i: apodization design and line element beamforming, IEEE Transactions on Ultrasonics, Ferroelectrics, and Frequency Control. 62 (2015) 947-958.